Influence of Alkyl Chain Length on the Crystal Structures and Optical SHG of *N*-*n*-Alkyl-2,4-dinitroanilines: Role of Dipolar and Dispersion Energies

P. Gangopadhyay and T. P. Radhakrishnan*

School of Chemistry, University of Hyderabad, Hyderabad 500 046, India

Received June 2, 2000. Revised Manuscript Received August 25, 2000

The length of alkyl chains attached to NLO chromophores exerts a critical control on their crystal structures and SHG capability. Systems with short as well as long alkyl chains form centrosymmetric lattices whereas those with chains of intermediate length, typically butyl chains, form noncentrosymmetric lattices and show SHG. Investigation of a series of *N*-*n*-alkyl-2,4-dinitroanilines is reported along with crystal structure analysis of the propyl, butyl, and pentyl derivatives. Packing energy calculations are carried out for the three structures. There are no intermolecular H-bonds in these crystals. The maximum values of dipole−dipole and dispersion energies in the set are found in the centrosymmetric crystals of the propyl and pentyl derivatives, respectively. Intermediate values of the two energy components are observed in the butyl derivative, which alone has a noncentrosymmetric crystal structure and is SHG active.

Introduction

Organized assembly of molecules to achieve specific material properties in the bulk state calls for a delicate balance between a variety of intermolecular interactions. π-Stacking with small interplanar spacing between open shell molecules promotes electrical conductivity in molecular solids.[1] Mutual disposition of ion radicals exerts a critical control on the spin density overlaps leading to ferro- or antiferromagnetism in organic magnetic materials.[2] Quadratic nonlinear optical (NLO) applications[3] necessarily require noncentrosymmetric materials, and a suitable alignment of the hyperpolarizability tensor components of the molecular chromophores gives rise to highly efficient systems.[4] Extensive computational and experimental explorations have led to the development of several classes of organic, organometallic, and metal coordination molecules possessing large hyperpolarizability.[5] Many methods have also been developed to assemble such molecules into efficient NLO materials. At the molecular level, techniques such as introduction of chirality,[6] internal cancellation of dipole components,[7] and incorporation of H-bonding features[8] have been extensively used. Presence of long alkyl chains usually bestows mesoscopic characteristics on molecular materials and is the hallmark of liquid crystal design. However, the incorporation of alkyl chains of appropriate length can influence the solid-state properties of crystalline materials as demonstrated in TTF-based semiconductors.[9] We have shown that the attachment of optimally long alkyl chains to NLO chromophores leads to noncentrosymmetric crystal lattices and optical second harmonic generation (SHG) capability. Diaminodicyanoquinodimethanes with alkyl chains of length 4, 5, and 6 were found to be SHG active while those with no alkyl chain or chains of length 3, 7, 8, and 12 were inactive.[10] Similarly, SHG activity is observed only in the butyl derivative among the various alkyl-chain-substituted 4-nitroanilines;[11] we have investigated this in detail through crystal structure analysis.[12]

Ab initio prediction of crystal structures of molecular materials continues to be a challenge. One of the focus of current efforts toward this goal is the rationalization

* Corresponding author. E-mail: tprsc@uohyd.ernet.in, Fax 91-40-301-2460, 91-40-301-0120.

(1) (a) Torrance, J. B. *Acc. Chem. Res.* **1979**, *12*, 79. (b) Torrance, J. B. *Mol. Cryst. Liq. Cryst.* **1985**, *126*, 55.

(2) McConnell, H. M. *J. Chem. Phys.* **1963**, *39*, 1910. (b) Allemand, P. M.; Srdanov, G.; Wudl, F. *J. Am. Chem. Soc.* **1990**, *112*, 9391. (c) Takahashi, M.; Turek, P.; Nakazawa, Y.; Tamura, M.; Nozawa, K.; Shiomi, D.; Ishikawa, M.; Kinoshita, M. *Phys. Rev. Lett.* **1991**, *67*, 746.

(3) Yariv, A. *Quantum Electronics*; John Wiley: New York; 1989; p 378.

(4) Chemla, D. S.; Zyss, J. *Nonlinear Optical Properties of Organic Molecules and Crystals*; Academic Press: New York; 1987; Vol. 1, p 23.

(5) Long, N. J. *Angew. Chem., Int. Ed. Engl.* **1995**, *34*, 21. (b) Zyss, J.; Nicoud, J.-F. *Curr. Opin. Solid State Mater. Sci.* **1996**, *1*, 533.

(6) Rieckhoff, K.; Peticolas, W. F. *Science* **1965**, *147*, 611. (b) Eaton, D. F. *Science* **1991**, *253*, 281. (c) Ukachi, T.; Sugiyama, T. *J. Opt. Soc. Am. B* **1993**, *10*, 1372.

(7) Zyss, J.; Chemla, D. S.; Nicoud, J.-F. *J. Chem. Phys.* **1981**, *74*, 4800. (b) Sigelle, M.; Zyss, J.; Hierle, R. *J. Non-Cryst. Solids* **1982**, *47*, 287.

(8) Desiraju, G. R. *Crystal Engineering: The Design of Organic Solids;* Elsevier: Amsterdam, 1989. (b) Bernstein, J.; Davis, R. E.; Shimoni, L.; Chang, N. *Angew. Chem., Int. Ed. Engl.* **1995**, *34*, 1555. (c) Ravi, M.; Gangopadhyay, P.; Rao, D. N.; Cohen, S.; Agranat, I.; Radhakrishnan, T. P. *Chem. Mater.* **1998**, *10*, 2371.

(9) Inokuchi, H. *Int. Rev. Phys. Chem.* **1989**, *8*, 95.

(10) Gangopadhyay, P.; Sharma, S.; Rao, A. J.; Rao, D. N.; Cohen, S.; Agranat, I.; Radhakrishnan, T. P. *Chem. Mater.* **1999**, *11*, 466. (b) Sharma, S.; Radhakrishnan, T. P. *Mol. Cryst. Liq. Cryst.* **2000**, *338*, 257.

(11) Chen, D.; Okamoto, N.; Matsushima, R. *Opt. Commun.* **1989**, *69*, 425.

(12) Gangopadhyay, P.; Rao, S. V.; Rao, D. N.; Radhakrishnan, T. P. *J. Mater. Chem.* **1999**, *9*, 1699.

10.1021/cm000446e CCC: $19.00
Published on Web 10/07/2000

of observed crystal structures. Even such limited exercises are often nontrivial due to the complex interplay of several intermolecular interactions that steer the formation of specific crystal architectures. In the context of quadratic NLO materials, the first level of insight to be gained is into the factors that favor the formation of centrosymmetric or noncentrosymmetric lattices. The unusual and fine control exerted by the alkyl chain length in this respect that we have described above merits careful examination. In the systems we have reported earlier the chain length dependence of the crystal lattice formation and the concomitant SHG activity were qualitatively ascribed to a subtle balance between dipole−dipole and nonpolar alkyl chain interactions. These systems also had extended intermolecular H-bonding interactions. In an attempt to obtain a quantitative appraisal of the factors related to the phenomenon, we have now investigated a series of alkyl derivatives of 2,4-dinitroaniline. These compounds were specifically chosen since they do not possess any intermolecular H-bond interactions; they possess only intramolecular H-bonds. These systems allow the isolation and examination of the remaining intermolecular interactions of which the primary ones are the electrostatic (Coulombic or dipole−dipole) interactions and nonpolar atom−atom dispersion forces. Another important consideration behind the choice of the 2,4-dinitroaniline system is that the parent system is known to be centrosymmetric[13] and hence SHG inactive. Interestingly, the observation of SHG in the butyl derivative of 2,4-dinitroaniline has been briefly reported.[14]

We present in this paper the synthesis and characterization of *N-n*-alkyl-2,4-dinitroanilines with the alkyl groups: propyl (**1**), butyl (**2**), pentyl (**3**), hexyl (**4**), and heptyl (**5**). Powder second harmonic generation studies show that only the butyl derivative is active. Crystal structures of **1**, **2**, and **3** are presented; these are in agreement with the SHG studies. Using well-known atom−atom potentials and molecular dipoles calculated using semiempirical and ab initio quantum chemical methods, we assess the relative contributions of dispersion and dipole−dipole energies to the packing potential energy in the three structures. The energy factors associated with the formation of the centrosymmetric and noncentrosymmetric crystal lattices are delineated.

Experimental Section

All the compounds were synthesized following the procedure reported in ref 15. The detailed procedure is described for **2**. A 1.00 g (4.93 mmol) sample of 1-chloro-2,4-dinitrobenzene was dissolved in 5 mL of dry, freshly distilled DMSO and cooled to 15 °C with vigorous stirring. A 2.80 g (20 mmol) sample of potassium carbonate was added to the solution and stirred. A 0.45 g (6.08 mmol) sample of *n*-butylamine was slowly added to the solution. The progress of the reaction was monitored by TLC; about 96% conversion was observed in 30 min. Stirring was continued for another 30 min. The reaction mixture was poured in 200 g of crushed ice and stirred vigorously. The yellow precipitate formed was filtered and washed with water. The filter cake was dried in air and purified by eluting through a basic alumina column using an ethyl acetate−hexane (20:80) mixture to produce 0.92 g (78% yield) of **2**. The product was further purified by recrystallization from methanol−water. Crystals were grown from toluene−chloroform (85:15) mixture. **1**, **3**, **4**, and **5** were synthesized similarly; the yields for the various compounds were 75−88%. **1**, **3**, and **4** were crystallized from toluene−chloroform. They were also recrystallized from ethyl acetate−hexane for the powder SHG experiments.

***N-n*-Propyl-2,4-dinitroaniline (1).** Mp: 100−102 °C; UV−vis (methanol): λ_{max} = 385 nm, $\lambda_{cut-off}$ = 458 nm. FT-IR (KBr pellet): ν/cm^{-1} = 3369.9 (N−H stretch), 3107.6, 2976.1 (C−H stretch), 1624.2 (aromatic C=C stretch), 1521.9, 1421.7, 1336.8 (NO_2 stretch). ^{1}H NMR ($CDCl_3$): δ/ppm = 1.1 (t, J = 7.5 Hz, 3H), 1.85 (sx, 2H), 3.4 (q, J = 6.5 Hz, 2H), 6.95 (d, J = 9.6 Hz, 1H), 8.2 (d, J = 9.5 Hz, 1H), 8.5 (s, 1H), 9.0 (d, J = 2.8 Hz, 1H). ^{13}C NMR ($CDCl_3$): δ/ppm = 11.37, 22.04, 45.28, 114.00, 124.19, 130.22, 135.84, 148.46. Elemental analysis (calculated for $C_9H_{11}N_3O_4$): % C = 48.12 (48.01), % H = 5.12 (4.92), % N = 18.63 (18.66).

***N-n*-Butyl-2,4-dinitroaniline (2).** Mp: 92−94 °C; UV−vis (methanol): λ_{max} = 385 nm, $\lambda_{cut-off}$ = 451 nm. FT-IR (KBr pellet): ν/cm^{-1} = 3362.2 (N−H stretch), 3107.6, 2959.1 (C−H stretch), 1624.2 (aromatic C=C stretch), 1521.9, 1419.7, 1334.8 (NO_2 stretch). ^{1}H NMR ($CDCl_3$): δ/ppm = 1.1 (t, J = 7.3 Hz, 3H), 1.55 (sx, 2H), 1.85 (qn, 2H), 3.4 (q, J = 6.2 Hz, 2H), 6.95 (d, J = 9.5 Hz, 1H), 8.2 (d, J = 9.6 Hz, 1H); 8.5(s, 1H), 9.0 (d, J = 2.7 Hz, 1H). ^{13}C NMR ($CDCl_3$): δ/ppm = 13.64, 20.10, 30.70, 43.34, 114.07, 124.11, 130.19, 135.76, 148.45. Elemental analysis (calculated for $C_{10}H_{13}N_3O_4$): % C = 50.40 (50.21), % H = 5.32 (5.44), % N = 17.18 (17.57).

***N-n*-Pentyl-2,4-dinitroaniline (3).** Mp: 78−80 °C; UV−vis (methanol): λ_{max} = 383 nm, $\lambda_{cut-off}$ = 447 nm. FT-IR (KBr pellet): ν/cm^{-1} = 3352.6 (N−H stretch), 3107.6, 2934.0 (aliphatic C−H stretch), 1622.3 (aromatic C=C stretch), 1520.0, 1423.6, 1338.7 (NO_2 stretch). ^{1}H NMR ($CDCl_3$): δ/ppm = 1.1 (t, J = 6.8 Hz, 3H), 1.3−1.7 (m, 4H), 1.85 (qn, 2H), 3.4 (q, J = 7.1 Hz, 2H), 6.95 (d, J = 9.6 Hz, 1H), 8.2 (d, J = 9.1 Hz, 1H); 8.5 (s, 1H), 9.0 (d, J = 2.1 Hz, 1H). ^{13}C NMR ($CDCl_3$): δ/ppm = 13.80, 22.23, 28.33, 28.98, 43.60, 114.12, 123.97, 130.11, 135.65, 148.41. Elemental analysis (calculated for $C_{11}H_{15}N_3O_4$): % C = 51.97 (52.17), % H = 5.97 (5.97), % N = 16.42 (16.59).

***N-n*-Hexyl-2,4-dinitroaniline (4).** Mp: 62−63 °C; UV−vis (methanol): λ_{max} = 384 nm, $\lambda_{cut-off}$ = 447 nm. FT-IR (KBr pellet): ν/cm^{-1} = 3362.2 (N−H stretch), 3107.6, 2959.1 (C−H stretch), 1624.2 (aromatic C=C stretch), 1521.9, 1419.7, 1334.8 (NO_2 stretch). ^{1}H NMR ($CDCl_3$): δ/ppm = 0.95 (t, J = 6.6 Hz, 3H), 1.2−1.6 (m, 6H), 1.85 (qn, 2H), 3.4 (q, J = 6.5 Hz, 2H), 6.95 (d, J = 9.6 Hz, 1H), 8.2 (d, J = 9.6 Hz, 1H), 8.5 (s, 1H), 9.0 (d, J = 2.8 Hz, 1H). ^{13}C NMR ($CDCl_3$): δ/ppm = 13.88, 22.46, 26.54, 28.63, 31.30, 43.64, 114.11, 124.04, 130.15, 135.76, 148.45. Elemental analysis (calculated for $C_{12}H_{17}N_3O_4$): % C = 53.06 (53.92), % H = 6.18 (6.41), % N = 15.33 (15.72).

***N-n*-Heptyl-2,4-dinitroaniline (5).** Mp: 25−28 °C; bp: 195 °C (2 mm Hg); UV−vis (methanol): λ_{max} = 385 nm, $\lambda_{cut-off}$ = 456 nm. FT-IR (KBr pellet): ν/cm^{-1} = 3329.4 (N−H stretch), 3036.2, 2928.2 (C−H stretch), 1628.1 (aromatic C=C stretch), 1535.5, 1437.1, 1338.8 (NO_2 stretch). ^{1}H NMR ($CDCl_3$): δ/ppm = 0.9 (t, J = 6.3 Hz, 3H), 1.2−1.7 (m, 8H), 1.9 (qn, 2H), 3.4 (q, J = 6.5 Hz, 2H), 6.95 (d, J = 9.6 Hz, 1H), 8.2 (d, J = 9.6 Hz, 1H); 8.5 (s, 1H), 9.0 (d, J = 2.9 Hz, 1H). ^{13}C NMR ($CDCl_3$): δ/ppm = 13.96, 22.52, 26.84, 28.68, 28.83, 31.61, 43.63, 114.13, 124.01, 130.12, 135.68, 148.41. Elemental analysis (calculated for $C_{13}H_{19}N_3O_4$): % C = 55.63 (55.51), % H = 6.92 (6.81), % N = 15.32 (14.94).

Second harmonic generation from microcrystalline powders was examined using the Kurtz−Perry[16] method. Particle sizes were graded using standard sieves; sizes ranging from 50 to 300 μm were studied. Samples were loaded in glass capillaries having an inner diameter of 600 μm. Fundamental beam (1064

(13) Prasad, L.; Gabe, E. J.; Lepage, Y. *Acta Crystallogr.* **1982**, *B38*, 674.

(14) Vizgert, R. V.; Davydov, B. L.; Kotovshchikov, S. G.; Starodubsteva, M. P. *Sov. J. Quantum Electron. (Engl. Transl.)* **1982**, *12*, 214.

(15) Twieg, R.; Azema, A.; Jain, K.; Cheng, Y. Y. *Chem. Phys. Lett.* **1982**, *92*, 208.

(16) Kurtz, S. K.; Perry, T. T. *J. Appl. Phys.* **1968**, *39*, 3798.

nm) of a Q-switched nanosecond-pulsed Nd:YAG laser (Continuum, model 660B-10) was used. The second harmonic signal was collected using appropriate optics and detected using a PMT (Hamamatsu), monochromator (Jobin-Yvon model HRS-2), and oscilloscope (Tektronix, model TDS 210, 60 MHz). Filters were used when needed, so that the signal measured on the oscilloscope was in the same range for all samples. Microcrystalline urea having particle size >150 μm was used as the reference in all SHG measurements. The SHG measured for a standard sample of *N*-4-nitrophenyl-(*S*)-prolinol (NPP) was 138 U (1 U = SHG of urea). The error in the measurements are ~10−15%.

X-ray diffraction data were collected on an Enraf-Nonius MACH3 diffractometer. Mo Kα radiation with a graphite crystal monochromator in the incident beam was used. Data were reduced using Xtal3.4;[17] Lorentz and polarization corrections were included. All non-hydrogen atoms were found using the direct method analysis in SHELX-97,[18] and after several cycles of refinement the positions of the hydrogen atoms were calculated and added to the refinement process. Graphics were handled using ORTEX6a.[19] Details of data collection, solution and refinement, fractional coordinates with anisotropic thermal parameters, and full lists of bond lengths and angles are submitted as Supporting Information.

Theoretical Methods

The packing potential energy of molecular crystals is usually estimated by adding the contributions from (i) repulsions between closed shell atoms, (ii) attraction between polarization induced instantaneous dipoles, (iii) Coulombic interaction between permanent atomic charges, and (iv) H-bond interactions.[20,21] In the present case we can omit the H-bond term since intermolecular H-bonds are excluded by design. The first two are computed using atom−atom potentials, and we refer to them together as the dispersion component, *D*.

$$D = \sum_{n} \sum_{i,j} [A \exp(-Br_{ij}) - C/r_{ij}^{6}]$$

i runs over the atoms of a reference molecule and *j* over those of the surrounding molecules, *n*, and r_{ij} is the distance between atoms *i* and *j*. We have employed the atom−atom potentials *A*, *B*, and *C* compiled by Gavezzotti and Simonetta.[20] Lattice summation of Coulomb interaction between atomic charges on molecules often runs into convergence problems.[20] We experienced this difficulty in our calculations as well, and the Coulomb energy sums are found to be very sensitive to the distance cutoff and the number of unit cells used. Hence, we have estimated the electrostatic energy component using the sum of dipole−dipole interaction energies, DD, between the molecular dipole vector of the reference molecule, μ_0, and of its neighbors, μ_n.[22]

$$\mathrm{DD} = \sum_{n} \{[(\mu_0 \cdot \mu_n)/r^3] - [3(\mu_0 \cdot \mathbf{r})(\mu_n \cdot \mathbf{r})/r^5]\}$$

r is the vector connecting the centers of the two dipoles, and *r* is its magnitude. The molecular dipole vectors (as well as atomic charges used in Coulomb energy calculations referred to above) were computed from semiempirical as well as ab initio calculations on molecular structures taken from the crystal structure. In the case of semiempirical computations, the H atoms alone were optimized keeping the non-H-atom framework intact since the C−H and N−H bonds from the X-ray analysis are too short. The AM1[23] procedure was used for the semiempirical studies, and the B3LYP/6-31G** level was employed in the ab initio calculations.[24] In the lattice energy calculations, the dipole vectors were positioned at the center of mass of the molecule. In the case of crystals having more than one molecule in the asymmetric unit, each one was taken in turn as the reference molecule and *D* and DD were computed. The data presented are the averaged values. The summation of the interaction energies starts with the second molecule (if present) in the asymmetric unit containing the reference molecule and is followed by the other molecules in the same unit cell, generated by the symmetry operations of the relevant space group. We have subsequently summed the contributions typically over 1200−2500 unit cells growing outward from the initial unit cell, to cover approximately 50 Å distance in every direction, and convergence was obtained in all instances well before 1000 unit cells were reached. Increasing the distance cutoff to 150 Å produced no noticeable change in the *D* and DD values. The *D* energies are reported in kJ/mol whereas the DD energies are reported in arbitrary units since the dielectric constant of the solid medium is not known. We assume that the variation of the dielectric constant between the three compounds is negligible. Since there is no unique protocol available to scale the values of the DD energies,[22] we confine our discussion to the trends of the energy components in the three structures. Complete computational results are submitted as Supporting Information.

Results and Discussion

The *N*-*n*-alkyl-2,4-dinitroanilines we have synthesized show a steady decrease in the melting point as the alkyl chain length increases; a similar trend was noticed in *N*-*n*-alkyl-4-nitroanilines[12] as well. The heptyl derivative, **5**, remains liquid at room temperature. **4** does not crystallize well, but single crystals of **1**, **2**, and **3** could be grown from a toluene−chloroform mixture; they are found to belong to the monoclinic space groups $P2_1/c$, $P2_1$, and $P2_1/c$, respectively. The crystallographic data are collected in Table 1. **1** has one molecule in the asymmetric unit, and **2** and **3** have two each. All the molecular structures show intramolecular H-bonding between the amino group and the ortho nitro group; the N···O distances range from 2.618 to 2.642 Å, and the N−H···O angles range from 128.8° to 131.2°. Within the

(17) Hall, S. R., King, G. S. D., Stewart, J. M., Eds.; Xtal3.4, University of Western Australia, 1995.
(18) Sheldrick, G. M. SHELX-97, University of Göttingen, 1997.
(19) McArdle, P. *J. Appl. Crystallogr.* **1995**, *28*, 65.
(20) Gavezzotti, A.; Simonetta, M. *Chem. Rev.* **1982**, *82*, 1.
(21) Pertsin, A. J.; Kitaigorodsky, A. I. *The Atom-Atom Potential Method*; Springer-Verlag: Berlin, 1987. (b) Gavezzotti, A. *J. Am. Chem. Soc.* **1991**, *113*, 4622.
(22) Gavezzotti, A.; Simonetta, M. *Acta Crystallogr.* **1976**, *A32*, 997.
(23) Dewar, M. J. S.; Zoebisch, E. G.; Healy, E. F.; Stewart, J. J. P. *J. Am. Chem. Soc.* **1985**, *107*, 3902.
(24) *Gaussian94*, Revision D.2: Frisch, M. J.; Trucks, G. W.; Schlegel, H. B.; Gill, P. M. W.; Johnson, B. G.; Robb, M. A.; Cheeseman, J. R.; Keith, T.; Petersson, G. A.; Montgomery, J. A.; Raghavachari, K.; Al-Laham, M. A.; Zakrzewski, V. G.; Ortiz, J. V.; Foresman, J. B.; Cioslowski, J.; Stefanov, B. B.; Nanayakkara, A.; Challacombe, M.; Peng, C. Y.; Ayala, P. Y.; Chen, W.; Wong, M. W.; Andres, J. L.; Replogle, E. S.; Gomperts, R.; Martin, R. L.; Fox, D. J.; Binkley, J. S.; Defrees, D. J.; Baker, J.; Stewart, J. P.; Head-Gordon, M.; Gonzalez, C; Pople, J. A.; Gaussian, Inc., Pittsburgh, PA, 1995.

Table 1. Crystallographic Data for 1, 2, and 3

	1	**2**	**3**
molecular formula	$C_9H_{11}N_3O_4$	$C_{20}H_{26}N_6O_8$	$C_{22}H_{30}N_6O_8$
formula weight	225.21	478.46	506.52
crystal system	monoclinic	monoclinic	monoclinic
space group	$P2_1/c$	$P2_1$	$P2_1/c$
a, Å	8.225 (3)	4.411 (8)	7.722 (12)
b, Å	11.3285 (13)	24.684 (11)	27.096 (5)
c, Å	11.2088 (18)	10.624 (5)	12.246 (5)
β, deg	97.04 (2)	94.16 (9)	99.59 (7)
Z	4	2	4
ρ_{calcd}, g cm^{-3}	1.443	1.377	1.332
μ, cm^{-1}	1.15	1.08	1.03
no. of unique reflections	2498	4086	5493
no. of reflections with	$I > 2\sigma_I$: 1357	$I > \sigma_I$: 3739	$I > \sigma_I$: 5218
no. of parameters	152	309	327
GOF	1.033	0.958	1.047
R (for $I > 2\sigma_I$)	0.0400	0.0588	0.0606
wR_2	0.0847	0.1736	0.2346

alkyl chains, the conformations are trans in all the cases. However, the conformation around the N−C bond connecting the amino group to the alkyl chain is gauche in **1**, trans in both the molecules in the asymmetric unit of **3**, and gauche and trans in the two molecules in the asymmetric unit of **2**.

The lattice packings in the three crystals are shown in Figures 1−3. In the centrosymmetric lattices of **1** and **3**, antiparallel alignment of the molecules or molecule pairs is clearly visible. In **2** the two molecules in the asymmetric unit, A and B (Figure 3), are oriented nearly orthogonal; the angle between the amino-*p*-nitro axes of the two molecules is 79.7°. The corresponding angles that A makes with A′ and B′ generated by the screw rotation operation are respectively 89.4° and 163.9°. The AM1/CPHF[25] calculation on *N*-*n*-butyl-2,4-dinitroaniline indicates a static hyperpolarizability of 8.03×10^{-30} esu, and the hyperpolarizability pseudo vector[26] is nearly coincident with the amino-*p*-nitro axis. On the basis of the relative molecular orientations within the A−B′ and B−A′ pairs, only a moderate SHG capability is expected in **2**. The powder SHG measured for different particle sizes of **2** are shown in Table 2. The SHG increases with particle size and saturates at an average value of 10.7 U for sizes >150 μm, indicating phase-matchable behavior. We have also checked **2** recrystallized from an ethyl acetate−hexane mixture; the saturation value of SHG is found to be 6.4 U. **1**, **3**, and **4** recrystallized from both solvent systems showed no SHG. **5** was checked at temperatures below its melting point; it produced no SHG. As noted earlier, the parent system with no alkyl chain is also SHG inactive.

The influence of alkyl chains on the crystal structure and hence on the SHG capability of the 2,4-dinitroanilines parallels what was observed in the 4-nitroanilines. Since no intermolecular H-bonds exist in the present series of molecules, we have examined the relative contributions of the dipole−dipole and dispersion energies to the crystal packing. Semiempirical AM1 (with H atom optimization) and ab initio calculations were carried out on the molecular structures extracted

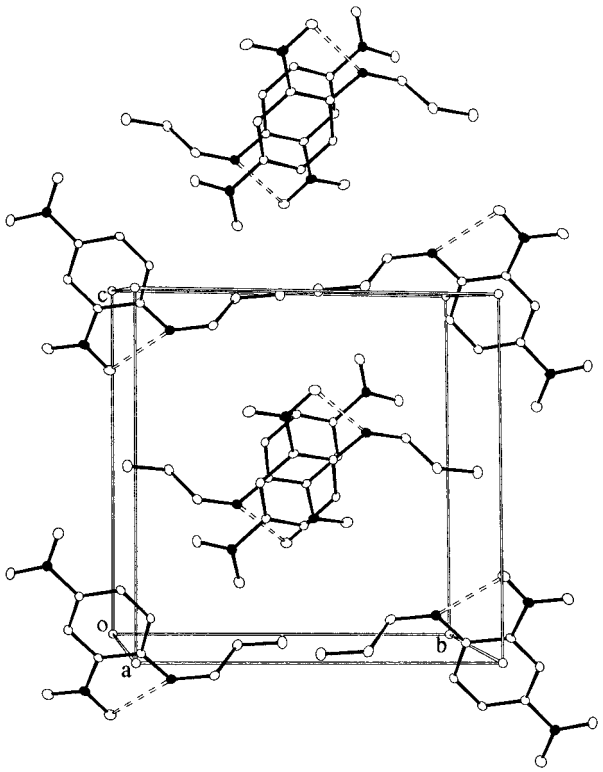

Figure 1. Crystal structure of **1**; H-bonds are shown as dashed lines. N atoms (●) are indicated; H atoms are not shown.

from the crystal structures of **1**, **2**, and **3**. The dipole vector computed from the AM1 procedure for **1**, **2**, and **3** are shown in Figure 4; the vector is positioned at the center of mass of the molecules. The ab initio calculated vectors are very similar in magnitude and orientation. For the packing energy computations of **1**, the single molecule in the asymmetric unit was set as the reference. The energies, *D* and DD, were computed as described earlier. In **2** and **3** we have carried out this exercise with each of the molecules in the asymmetric unit taken as the reference. The growth and convergence of the energy components as the unit cells are added are illustrated in Figure 5; the data shown is that of **2** with molecule B (Figure 2) as the reference and the DD calculated using the ab initio dipole vector. Similar results are obtained with the geometries and dipoles from the AM1 partial optimization calculation. *D* and DD energies converge within about 500−1000 unit cells for all the structures. The summation of Coulomb energies between the atomic charges showed a complex oscillatory behavior in most of these systems. The converged dipole−dipole and dispersion energy components for the three crystals having alkyl chains of length 3, 4, and 5 are illustrated in Figure 6. The energies computed using the dipoles and partially optimized geometries from AM1 as well as the dipoles from ab initio computations are found to agree closely with each other. Figure 6 shows that the dispersion energy contribution to the crystal stabilization increases smoothly as the alkyl chain length increases. However, the dipole−dipole energy contributions are found to decrease.

The increase of dispersion energy from **1** to **3** is a direct consequence of the increasing chain length and the associated molecular size. The dipole−dipole inter-

(25) Kurtz, A. J.; Stewart, J. J. P.; Dieter, K. M. *J. Comput. Chem.* **1990**, *11*, 82. (b) Kanis, D. R.; Ratner, M. A.; Marks, T. J. *Chem. Rev.* **1994**, *94*, 195.

(26) Sharma, S.; Gangopadhyay, P.; Swathi, A.; Radhakrishnan, T. P. *Phys. Chem. Chem. Phys.* **2000**, *2*, 1147.

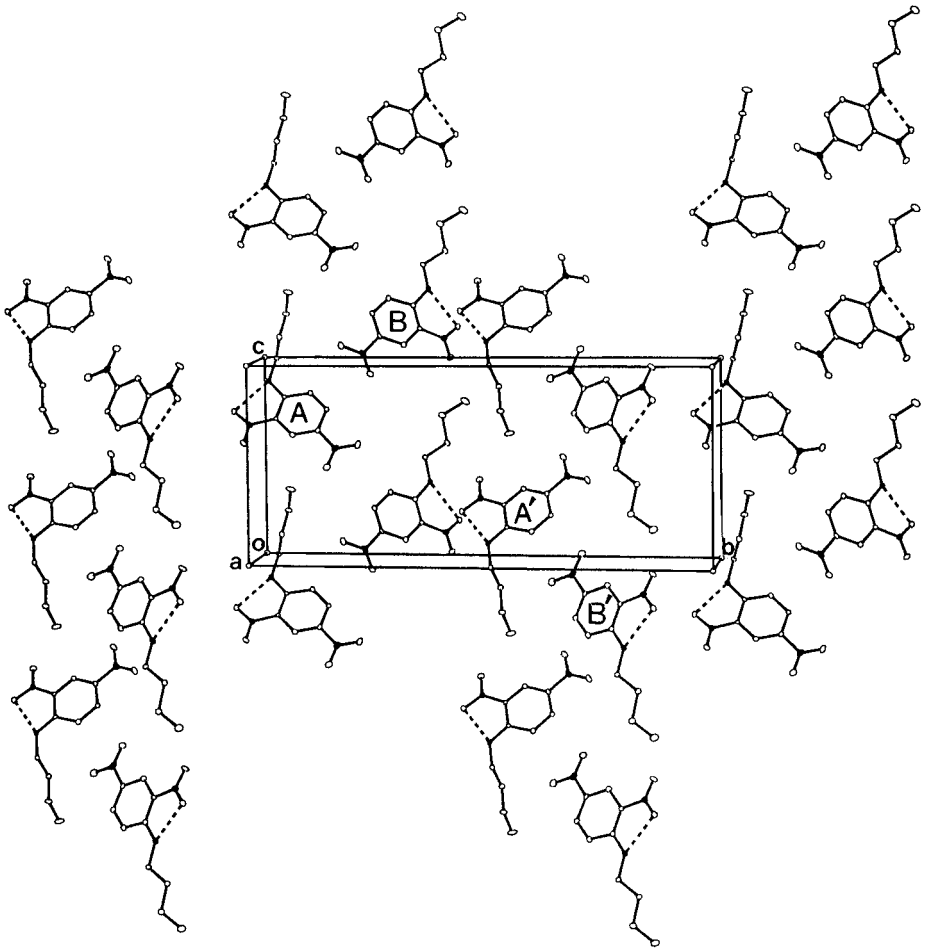

Figure 2. Crystal structure of **2**; H-bonds are shown as dashed lines. N atoms (●) are indicated; H atoms are not shown. See text for discussion on the molecules A, B, A′, and B′.

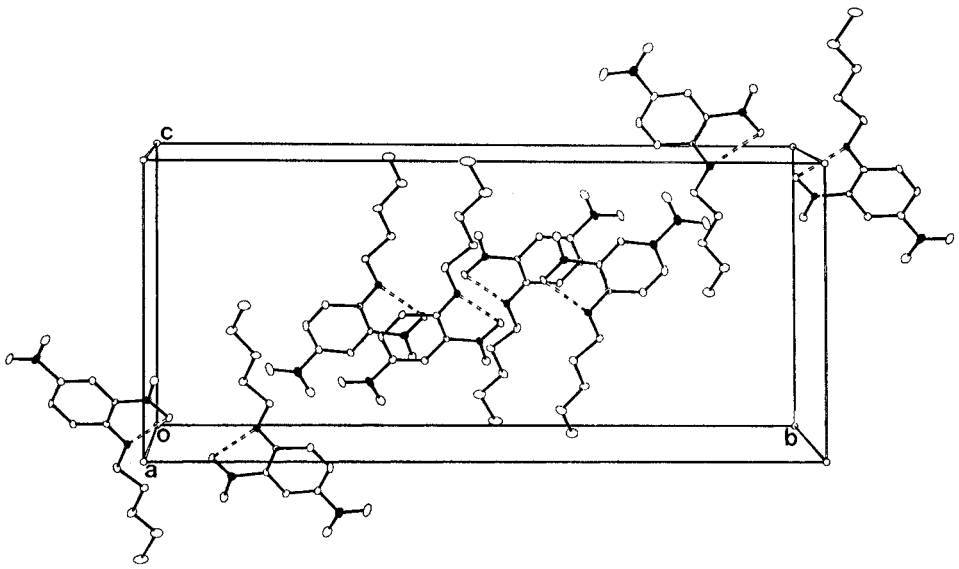

Figure 3. Crystal structure of **3**; H-bonds are shown as dashed lines. N atoms (●) are indicated; H atoms are not shown.

actions are dominated by the 2,4-dinitroaniline moiety where most of the atomic charges reside and are expected to be independent of the alkyl chain length. However, as the chain length increases, the molecular volume increases. In the crystals of a homologous series such as **1**, **2**, and **3**, the molecular volume increase is likely to cause a parallel increase in the average intermolecular distances. This appears to be the case as indicated by the distance between the centers of mass of the closest molecules in **1**, **2**, and **3** which are respectively 3.950, 4.411, and 4.795 Å. Further, the nearest-neighbor molecules in **1** are oriented antiparallel favoring dipole−dipole attraction whereas the nearest neighbors in **2** and **3** are parallel. (The center of inversion in **3** relates the nearest-neighbor pair with a similar pair oriented antiparallel). The two factors of

Table 2. Powder SHG (Relative to That of Urea of Particle Size >150 μm) of 2 Recrystallized from (a) Chloroform−Toluene and (b) Ethyl Acetate−Hexane Mixtures as a Function of Particle Size

particle size range (μm)	SHG/U (a)	SHG/U (b)	particle size range (μm)	SHG/U (a)	SHG/U (b)
50−75	-	3.0	120−150	-	5.5
50−90	2.0	-	150−180	11.9	5.5
75−90	-	4.0	180−200	9.9	6.0
90−100	4.0	4.5	200−250	9.9	7.0
100−120	-	5.5	250−300	10.9	7.0
100−150	7.9				

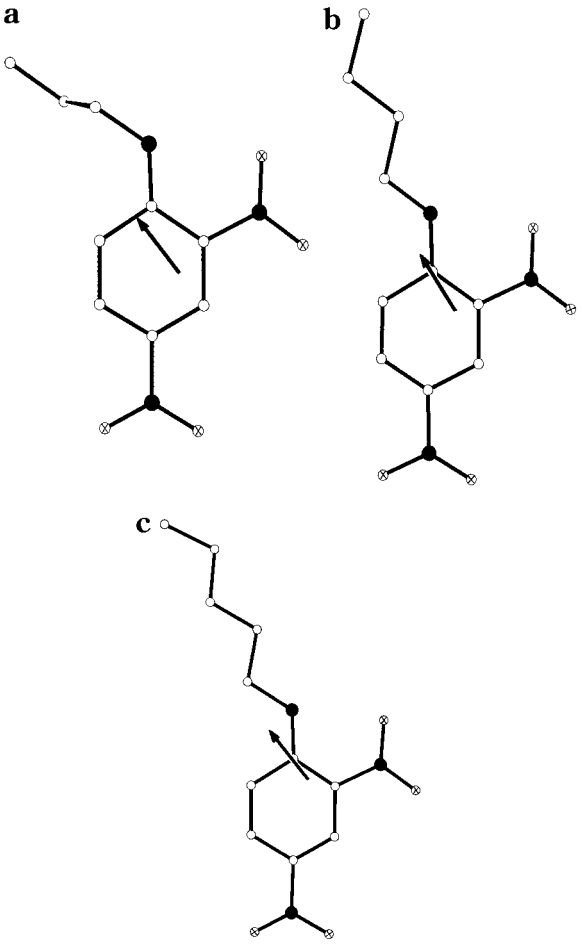

Figure 4. Molecular structure extracted from crystal structure of (a) **1**, (b) **2**, and (c) **3**, showing the AM1 computed dipole vector at the center of mass of the molecule. In **2** and **3** only one molecule in the asymmetric unit is shown. N (●) and O (⊗) atoms are indicated; H atoms are not shown.

intermolecular distances and the orientation of neighboring molecules explain the decrease in the dipole−dipole interaction energy from **1** to **3**. In agreement with qualitative suggestions made earlier,[10,12] centrosymmetric packing arrangement is associated with the higher values of dipole−dipole or dispersion energy component, the former being the case with the propyl derivative and the latter with the pentyl derivative in the present set. The noncentrosymmetric lattice of the butyl derivative on the other hand exhibits an intermediate value of both energy factors. The alkyl chain length functions as a convenient handle to fine-tune these energy components.

We have carried out a similar investigation on the set of 4-nitroanilines reported earlier[12] using ab initio calculated dipole vectors. Once again as the alkyl chain

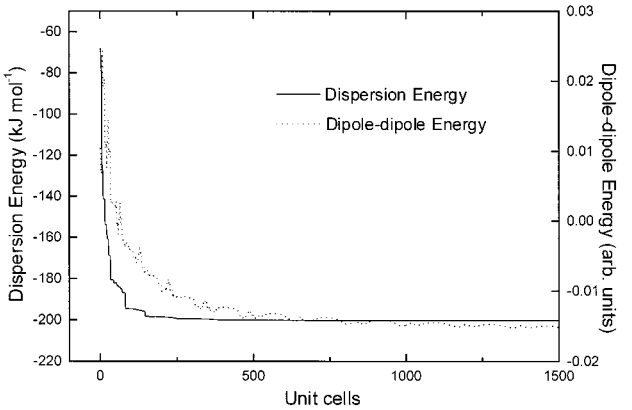

Figure 5. Convergence of the dipole−dipole and dispersion energies of **2** as contributions from neighboring unit cells are added; the energies are computed using the molecular structure extracted from the crystal structure and the dipole vectors from ab initio computations.

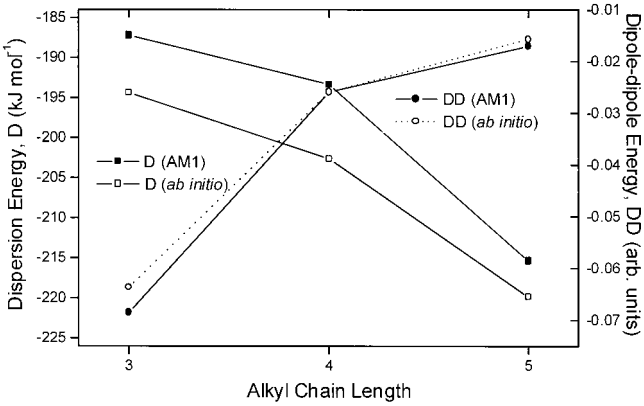

Figure 6. Computed dipole−dipole and dispersion energies of **1**, **2**, and **3** plotted against the respective alkyl chain lengths. Molecular structure extracted from crystal structure as well as from AM1 partial optimization and dipole vectors from ab initio and AM1 methods are used.

length increases from propyl to pentyl, the dispersion energy stabilization shows a steady increase; the respective values are −157.7, −173.5, and −195.4 kJ/mol. The dipole−dipole energy contribution decreases from propyl to butyl derivative, but then shows a marginal increase in the pentyl derivative; the values are −0.070, −0.027, and −0.033, respectively. We believe that the intermolecular H-bonding in these systems complicates the issue; however, the general trends are similar to those found in 2,4-dinitroanilines.

Conclusions

We have investigated the powder SHG capability of *N*-*n*-alkyl-2,4-dinitroanilines. As observed in the 4-nitroaniline series, only the butyl derivative is active. Crystal structure analysis of the propyl, butyl, and pentyl derivatives shows that the butyl derivative alone is noncentrosymmetric. These systems form a convenient test set to examine the relative contributions of dipole−dipole and dispersion energies to crystal packing, without complications arising from other intermolecular interactions such as H-bonding. Semiempirical and ab initio computations were used to estimate the atomic charges and dipole vectors of the molecules with the geometries from the crystalline state. Packing energy calculations reveal increasing stabilization due

to dispersion energies and decreasing stabilization due to the dipole−dipole energies as the chain length increases from 3 to 5. These observations suggest a possible balance between the dipole−dipole and dispersion energy components occurring at the intermediate chain length associated with the formation of the noncentric lattice. Efforts are under way to extend similar analysis to other families of alkyl-chain-substituted dipolar molecules. Insight gained from such explorations will be useful in developing the alkyl chain length as a simple and effective design element for molecular quadratic NLO materials.

Acknowledgment. Financial support from the Department of Science and Technology (Swarnajayanti Fellowship) and the use of the National Single Crystal Diffractometer Facility funded by the DST at the School of Chemistry, University of Hyderabad, are gratefully acknowledged. P.G. thanks the University Grants Commission for a Senior Research Fellowship. We thank Mr. P. Sharma for help with some of the computations.

Supporting Information Available: X-ray structure determination and crystal structure details and detailed computational results. This material is available free of charge via the Internet at http://pubs.acs.org.

CM000446E